

New Developments in Amorphous Silicon Based Microchannel Plates

Samira Frey, Luca Antognini, Mohammad Beygi, Christophe Ballif and Nicolas Wyrsh

Abstract—Microchannel plates fabricated from hydrogenated amorphous silicon (AMCPs) are a promising alternative to conventional glass microchannel plates. Their main advantages lie in their flexible fabrication processes, allowing for adaptable channel shapes and the possibility of vertical integration with an electronic readout, a tunable resistivity of the main amorphous silicon layer, which allows a charge replenishment by a current flowing directly through the bulk material and possibly a lower cost of production. In this publication, we present further developments of the AMCP technology and its characterization. Small channel diameters down to 1.6 μm could be achieved, resulting in an aspect ratio of 25. This led to an increase of the electron multiplication gain to 1500 compared to the previous maximum of 100. The fabricated devices were characterized under both continuous and pulsed illumination. Additionally, the gain dynamics were measured over several minutes, showing increased gain stability with respect to previous devices. With the achieved gain values of this new generation of AMCPs, this technology can now be considered a viable option for real applications such as time-of-flight positron emission tomography or mass spectrometry.

Index Terms—Amorphous Silicon, Deep Reactive Ion Etching, Microchannel Plates, Monolithic Integration, Spatial Resolution, Time Resolution, Particle Detection, Plasma-enhanced Chemical Vapor Deposition, Vacuum Detectors

I. INTRODUCTION

MICROCHANNEL plates (MCPs) are electron multipliers that were first introduced in the 1970's [1]. Nowadays, they are used in many applications, most notably for image intensifiers, mass spectrometry, astrophysics, and electron microscopy. Their main advantages over other detectors, such as silicon photomultipliers (SiPMs), lie in their fast timing characteristics (transit time spread is typically in the order of 10–20 ps for small pore diameters [2]), high spatial resolution and low background noise (≤ 0.1 counts cm^2s^{-1} [3]). MCPs are conventionally fabricated by fusing glass fibers. To achieve an emissive surface for the electron amplification, the glass capillary array can then be heated in the presence of hydrogen, leading to a chemical reduction of the channel surface. In a more recent manufacturing technique, resistive and emissive layers are deposited on the channel walls by atomic layer deposition (ALD), allowing for greater flexibility in the choice of the glass substrate, resistance, and emissive properties [4]. Despite the MCP technology having reached maturity, there

is still the aspiration to push the detector performance further - namely in the form of an increase in detection efficiency, time and spatial resolution, dynamic range, background counts, or detector size. An alternative approach to MCPs using hydrogenated amorphous silicon (a-Si:H) as a substrate was first explored in 2010 [5]. These a-Si:H based MCPs (AMCPs) exhibit some advantages over their glass counterparts. They can be fabricated directly on top of a wide range of substrates, most notably allowing for monolithic integration with readout electronic circuits. This minimizes the detector dead area and improves both the spatial and temporal resolution of the complete detector architecture. The conductivity of the a-Si:H material depends on the deposition conditions and can be varied by doping over several orders of magnitude. The charges extracted from the material during a multiplication event can therefore be directly recovered by a current flowing through the bulk material without the need for an additional conductive layer on the channel walls. At the same time, the resistance of the a-Si:H stack is still high enough to apply high bias voltages. This tunable resistivity of the amorphous silicon layer also opens the possibility of varying the resistance along the length of the channels by gradually adjusting the process parameters during the growth of the layer. Like this, the vertical resistivity and, therefore, the electric field could be optimized, which could help to alleviate or even eliminate saturation effects, hence allowing for high detector count rates [6]. Finally, AMCPs are fabricated using (micro-)fabrication techniques already optimized by the silicon or MEMS industry, making manufacturing potentially cheaper than glass MCPs. The fabrication techniques employed additionally allow for a fully customized channel geometry. After the initial proof of concept presented in 2014 [7], AMCPs have been continuously further developed [8]. This publication presents the optimized fabrication procedure and performance evaluation of the latest generation of AMCPs.

II. AMCP FABRICATION

AMCPs are manufactured using micromachining techniques, namely plasma-enhanced chemical vapour deposition (PE-CVD), photolithography, and deep reactive ion etching (DRIE). We only summarized the main fabrication steps, as detailed descriptions were already given in previous publications [7], [8]. The main a-Si:H multiplication layer is grown by a PE-CVD process, optimized to obtain thick layers (40–100 μm) with low intrinsic stress (≤ 10 MPa) and without structural defects, allowing to later apply strong electric fields over the AMCP. A grounded chromium-based intermediate

Manuscript received XX XX, 2023. This work was supported by the Swiss National Science Foundation (SNSF) under the Sinergia project on MEMS based Gamma Ray Detectors for Time-of-Flight Positron Emission Tomography (Grant number: 177165). All authors are with the Photovoltaics and Thin-Film Electronics Laboratory, Institute of Electrical and Micro Engineering (IEM), Ecole Polytechnique Fédérale de Lausanne (EPFL), Neuchâtel, Switzerland (Correspondence: samira.frey@bluewin.ch).

electrode is used to evacuate the leakage current flowing through the stack. It is separated from the bottom electrode by an a-Si:H decoupling layer. The thickness of this decoupling layer can be varied between 2–4 μm , which mainly affects the output capacitance of the final device. The channels are etched into the a-Si:H layer by a tailored Bosch process, using the metallic top electrode (either aluminium or chromium) as a hard mask. In the current fabrication process, the lower limit of the channel diameters is mainly given by the resolution limit of the photolithography process (between 800 nm to 1.2 μm depending on the exact design). Additionally, parameter control of the Bosch process becomes increasingly more critical with smaller channel diameters. Currently, the smallest pore diameter that could be realized in a working device is 1.6 μm . The channels on the AMCPs are arranged in a hexagonal pattern with minimum pitches of 3 μm (center-to-center) needed to ensure the structural stability of the thick a-Si:H layer. The AMCP test structures are grown on a single anode for each sensor area. Note that in possible future applications, the AMCPs could be directly grown on top of a readout circuit. The chips fabricated for testing purposes have sensor areas between 250 μm by 250 μm to 1000 μm by 1000 μm , which could be easily scaled up if required for a given application. A few adjustments have been made in the fabrication process with respect to the previous generation presented in [8]. The earlier $\mu\text{-Si}$ intermediate electrode has been replaced by a chromium-based one. This increased the conductivity of this electrode, preventing a voltage rise during a multiplication event. This also provided a better interface for the growth of the thick a-Si:H layer above it, reducing hydrogen accumulation and subsequent bubble formation. The diameters of the channels were also reduced from the previous minimum of 3 μm down to 1.6 μm . Fig. 1 shows a scanning electron microscope image of an AMCP cross-section. The sample shown in this image had a main channel length of 40 μm and an average channel diameter of 1.6 μm , resulting in an aspect ratio of 25.

III. MEASUREMENT SETUP AND PROCEDURES

A custom-built setup was used to determine the multiplication gain of the AMCPs under similar conditions to possible detector applications. Fig. 2 shows a schematic of the setup. The device to be tested was bonded to a double-sided interface board and placed on a rotatable support rod inside a vacuum chamber. A rotary dry pump and a turbomolecular pump allowed reaching a residual pressure of 5×10^{-6} mbar. Two feed-through connectors were implemented to provide the electrical connections. Two different illumination sources were used for the characterization, both operated at a normal incidence on the AMCP chip. A Pen-Ray mercury-vapour lamp provided continuous light with the main emission peak at 254 nm. The light could enter the vessel through an optical window made of fused silica. A pulsed laser (Nd:YAG) with a wavelength of 266 nm, a pulse duration of 7 ns (FWHM), and a tunable repetition rate between 1 to 4 kHz was used for testing the AMCP behavior in the transient regime. A photocathode, consisting of a 16 nm thick gold layer, was

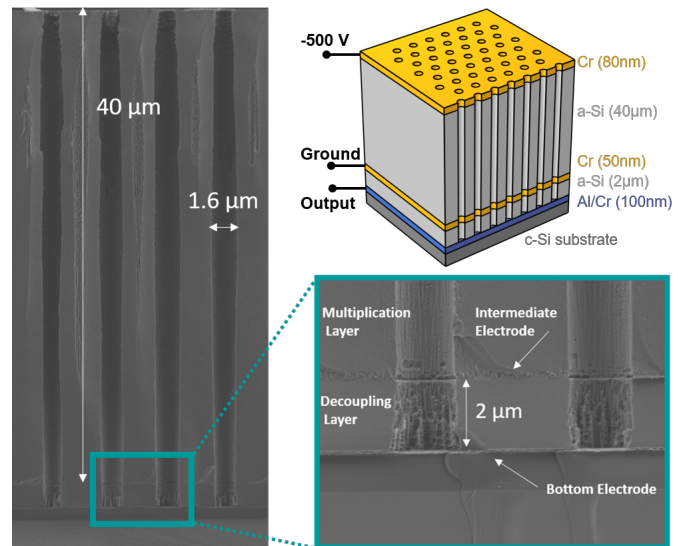


Fig. 1. Left: Cross-section image of AMCP channels. The channels have a length of 40 μm (from the top to the intermediate electrode where the electric field is applied) and an average channel diameter of 1.6 μm , resulting in an aspect ratio of 25. Note that the slight cone-shaped appearance is due to the difficulty of cleaving the samples straight through the center of the pores. Bottom right: Zoom of the lower part of the channel, highlighting the 2 μm thick decoupling layer. Top right: Schematic cross-section for comparison.

placed above the AMCPs at a distance of around 2 mm. Photons arrive on one side of this thin semitransparent layer and photoelectrons are emitted on the other side, towards the AMCP. The choice to use gold as a photocathode was motivated by its longevity and stability in air, despite the low measured quantum efficiency of around 0.0014 % at 254 nm. A thin metal plate with an opening in the middle, used as a photoelectron screen (or mask), was placed between the photocathode and the AMCP to restrict the photoelectron beam to the sensor area, and avoid parasitic collection by the wires bonded on the device. A potential difference could be applied between the photocathode and the top electrode to accelerate the generated photoelectrons towards the AMCP. To ensure a homogeneous electric field, the photoelectron screen bias was set at half the bias voltage between the AMCP and the photocathode using a voltage divider. A Stanford Research Systems PS310 high-voltage supply provided the voltage for the photocathode and the photoelectron screen. A Keithley 617 picoammeter supplied the bias voltage for the AMCPs. The anode signal was then measured either by the same picoammeter for the measurements under continuous illumination or with an oscilloscope (Teledyne LeCroy WaveSurfer 510) for the pulsed measurements using a 1 M Ω impedance input.

Before the gain of the AMCPs could be evaluated, the incoming electron flux from the photocathode needed to be calibrated. For this, a test sample consisting of several metal pads of same areas as the AMCP sensors was used (Fig. 2 (b), right). The photocathode was then illuminated, and the current arriving on the different pads was measured as a function of the applied bias between the photocathode and the metal pads.

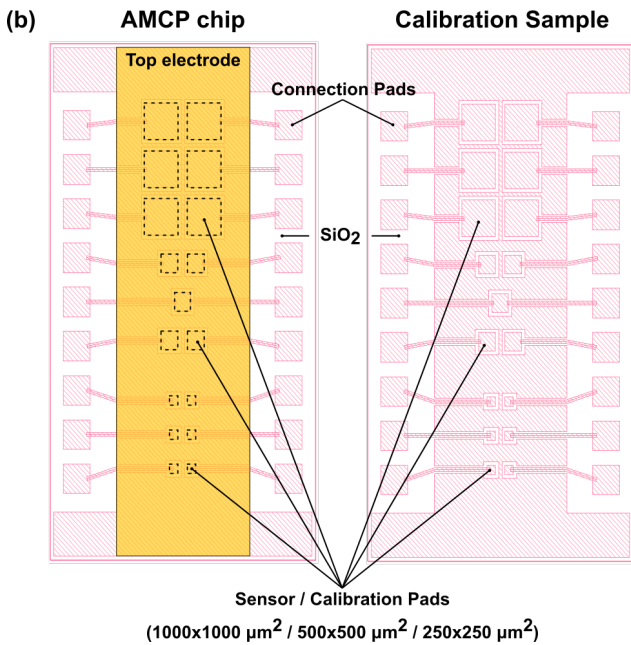
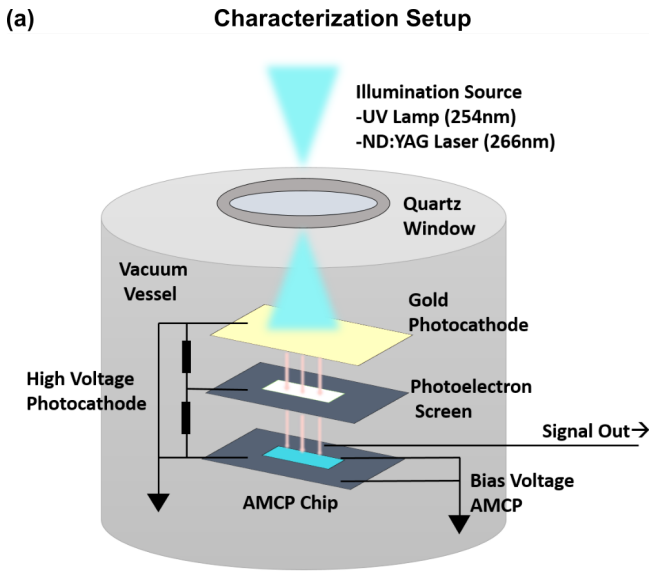


Fig. 2. (a) Schematic of the characterization setup. The test chip is placed inside a vacuum chamber with an optical window on top. A thin gold layer (16 nm) is used as a photocathode and placed above the bonded chip. Either a mercury lamp or a pulsed laser is used as illumination source, operating at a normal incidence on the AMCP. A photoelectron screen is used to restrict the illumination to the sensor area. A bias voltage can be applied to the AMCP top electrode and the photocathode. (b) Top view schematic of an AMCP chip and the calibration sample used to measure the flux of the photocathode. The sensors and the calibration pads have the same area and are made of the same metal.

The applied electric field helped to steer the photoelectrons onto the pads. A constant electron flux of $(1.70 \pm 0.05) \times 10^{13}/(\text{m}^2 \text{s})$ was measured under continuous illumination with the mercury lamp for voltage differences between 100 V and 500 V.

Once the incoming flux had been properly calibrated, the gain was then defined as the ratio between the output current (I_{Out}) and the incoming photoelectron flux (I_{In}) times the ratio of the area of the channels over the total sensor area, also called open area ratio (OAR), of the device. Then, the resulting gain was computed as

$$Gain = \frac{I_{Out}}{I_{In} \cdot OAR} \quad (1)$$

and represents the average multiplication factor of a single channel. The gain calibration for measurements in the transient regime with the pulsed laser was performed similarly using the oscilloscope (where the measured voltages are proportional to the current). The incoming photoelectron signal V_{In} was calibrated by measuring the voltage drop per laser pulse on the calibration pad while ensuring that the laser pulse evenly illuminates the entire pad area. The gain is then given by the ratio of the outgoing signal V_{Out} of the AMCPs and the incoming signal multiplied by the OAR

$$Gain = \frac{V_{Out}}{V_{In} \cdot OAR} \quad (2)$$

IV. AMCP CHARACTERIZATION

A. Gain dependence on the first impact energy

The working principle of AMCPs is based on secondary electron emission (SEE). SEE occurs in all materials when an incoming particle impinges on its surface. The total electron yield (TEY), that is the average number of electrons emitted per incident primary particle, depends on many parameters such as energy and incident angle of the incoming particle, energy losses of the secondary electrons inside the material, the potential barrier at the vacuum surface as well influences of the surface morphology. It is clear from looking at the avalanche process in AMCPs and MCPs alike that the TEY at the first impact can significantly affect the resulting gain. TEY of a-Si:H layers as a function of the energy of the incoming electrons has been studied by Löffler *et al.* [8] and showed a maximum yield for an energy of around 220 eV at normal incidence. In Figure 3, the AMCP gain was measured as a function of the incident photoelectron energy by varying the potential difference between the photocathode and the AMCP top electrode. From this, a broad maximum could be observed between 120 eV to 200 eV where the gain was roughly 20% higher than outside this range. This maximum yield appears to be shifted to lower energies compared to the findings in [8]. A reasonable explanation for this shift is that the majority of the electrons do not collide directly at the channel entrance but somewhat further down since the channels do not have a bias angle relative to the surface normal. Consequently, these electrons are then accelerated by the applied electric field over the AMCP until their first collision with the channel wall. Therefore, the potential difference between the photocathode and the AMCP top electrode underestimates the average collision energy of the incoming electrons. Another factor to consider is that the surface morphology of the channel walls is very different from that of the measured flat samples. Although a sample with higher roughness was also measured

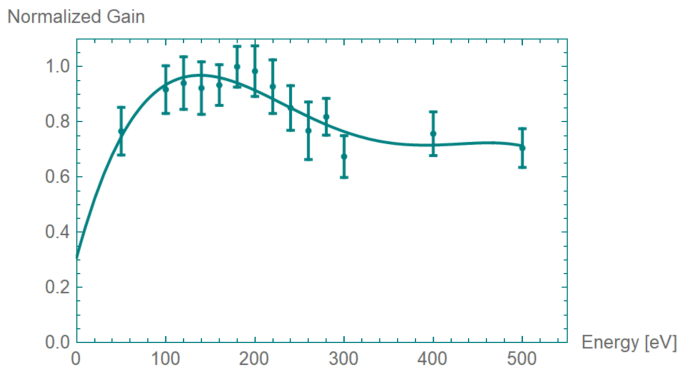


Fig. 3. Dependence of the measured gain on the acquired energy of the photoelectrons between the photocathode and the AMCP top electrode. A broad maximum between 120 eV to 200 eV was observed.

in [8] and showed an even higher optimum energy due to the variation of incident angles, this might not necessarily be a good representation of the surface inside a channel. For all the following gain measurements, the bias between AMCP and photocathode was set to 200 V to achieve the highest gain while maintaining a stable flux of electrons from the photocathode. This optimum potential difference may differ for samples with wall coatings and other channel geometries and must be readjusted in those cases.

B. Average channel gain

After calibration of the incoming flux and optimization of the first impact energy, the gain was then measured as a function of the applied AMCP bias voltage. The channel gain was evaluated under both continuous and pulsed illumination. Before each measurement, the samples were annealed for 30 minutes at 90 °C to ensure stable working conditions [9]. Additionally, a waiting period of around 10 minutes was kept after each change in the bias voltage. This was done because in materials with a large density of localized bandgap states (such as a-Si:H), a certain time is needed to ensure a new equilibrium of trapped carriers after a change in the electric field [10]. The gain was again calculated as the ratio between the anode current and the calibrated input current as defined above. Fig. 4 shows the recorded output signals in response to a laser pulse for bias voltages between -50 V to -500 V, following the expected exponential increase in signal with higher biases [11]. Note that the width of the signal is directly related to the long pulse duration of our laser (7 ns). The measured sample "MCP152" had an aspect ratio of 25 and channel lengths of 40 μm. Fig. 5 shows the calculated gain for the same "MCP152" sample as a function of the applied electric field corresponding to the used bias voltage. A maximum gain of around 1500 (1460 ± 54 under continuous illumination and 1494 ± 85 under pulsed illumination) was measured for an applied bias of -500 V (corresponding to an electric field of 12.5×10^4 V/cm given the a-Si:H layer thickness of 40 μm). Four pads with different sensor areas were measured in total, two of 250 μm by 250 μm and two others of 500 μm by 500 μm. The largest pads (1000 μm by 1000 μm) were excluded from the measurements - partially

because of some localized defects, where a few holes were missing in parts of the area, and because the laser spot did not uniformly illuminate the whole area. No dependence of the gain on the sensor area was observed. Also, no significant difference was observed between the measurements under continuous and pulsed illumination at high-bias voltages and strong electric fields. At lower biases, however, a difference in gain can be observed between the two illumination modes, with higher gain values in the pulsed regime. This discrepancy could be due to a measurement uncertainty or potentially be related to charging effects of the decoupling stack. The biggest uncertainty in the average channel gain measurements stems from the calibration of the incoming current. As described previously, a calibration sample was used to measure the flux of incoming photoelectrons. The calibration pad was fabricated with the same metal composition and thickness as the top electrode since the metal also produces a certain number of photoelectrons under illumination, which must be considered. To obtain the incoming current that enters the channel, the measured flux is scaled by the OAR of the device, as mentioned in section 3. This assumption might not be entirely accurate as particles impinging close to the edge of the channel could still be able to enter the latter and contribute to the avalanche. Additionally, the electric field might not be homogeneous close to the edge of the channels, changing the flux locally. However, the resulting systematic error cannot be easily quantified at present. However, the important conclusion that can be made from the measurements presented here is the considerable increase in gain from 100 [12] to 1500 in comparison to the previous generation of AMCPs. Another problem arises due to the fact that the photocathode appeared to get damaged under laser illumination, causing a decrease in its quantum efficiency over time. For this reason, the incoming signal was calibrated before and after measurements under pulsed illumination, and the photocathode had to be replaced at regular intervals.

The setup could be further upgraded to increase the accuracy of future measurements. For example, a conventional glass MCP installed between the photocathode and the AMCP would provide a larger incoming flux, reducing the measurement error since the number of photoelectrons produced on the AMCP itself would be significantly smaller than the electron flux stemming from the MCP. Additionally, this would allow us to test the AMCP response as a function of the incoming current and investigate the onset of saturation effects that still need to be observed.

C. Gain stability over time

The AMCP output current was measured under continuous illumination over several minutes to investigate its stability over time. The device was biased with -500 V, and the resulting current was recorded with a picoammeter. The measurement is shown in Fig. 6. The current first increases over several minutes before reaching a maximum and then slowly decreases again to finally stabilize after a few minutes. Once a stable current has been reached, it could be reproduced when the illumination was switched off and back on again. The gain

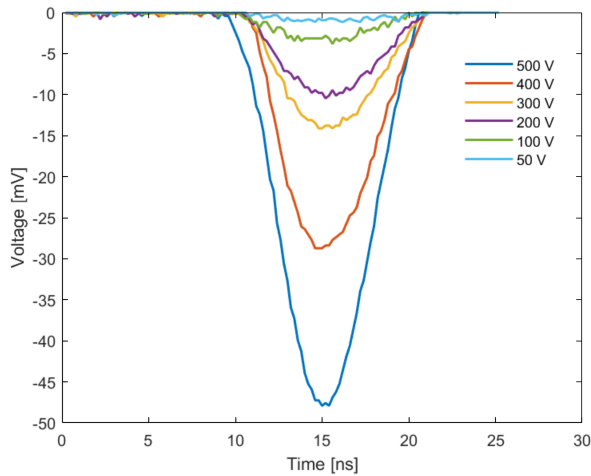


Fig. 4. Recorded output signals in response to a laser pulse with a pulse duration of 7 ns (FWHM). The signal was recorded for bias voltages between -50 V to -500 V. The recordings have been overlapped in the graph to demonstrate the increase in signal with higher AMCP bias.

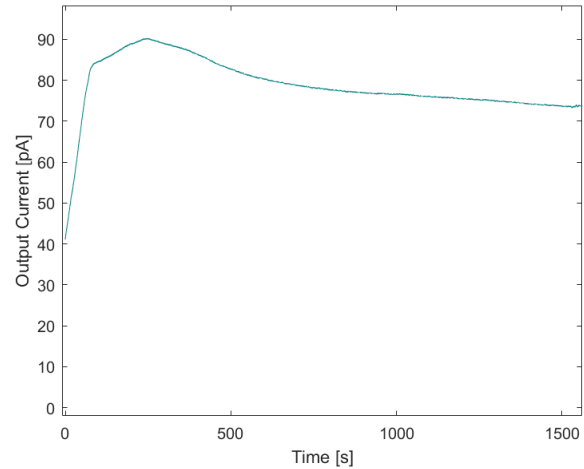


Fig. 6. Measured output current dynamics over several minutes (sensor area of 250 μm by 250 μm). The output current initially increases and then decreases again before eventually stabilizing after about 10 minutes.

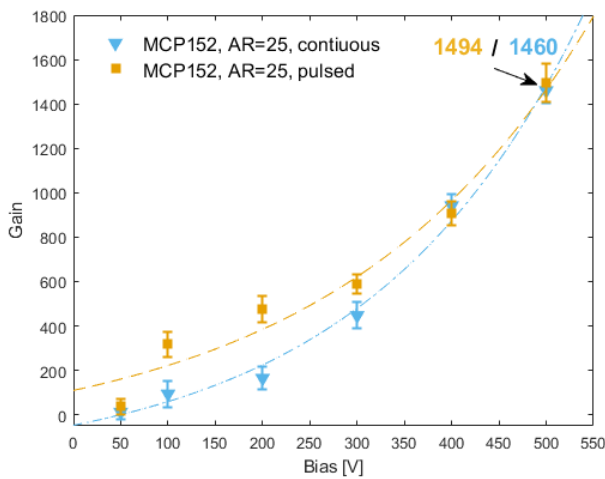


Fig. 5. Average channel gain of an AMCP with an aspect ratio of 25 measured as a function of the applied bias between top and middle electrodes (in absolute value). Dashed-lines are guides-to-the-eye. The gain was evaluated both under continuous illumination using a mercury lamp and under pulsed illumination with a laser source. A maximum gain of around 1500 (1460 ± 54 under continuous illumination and 1494 ± 85 under pulsed illumination) was measured for an applied electric field of $12.5 \cdot 10^4 \text{ V/cm}$.

dynamics can be explained in the following way - the first quick increase of the current over a few seconds is only due to the manual removal of the light shutter and is not related to the AMCP behavior. The following slower current increase could be tentatively explained by the presence of a residual water film on the channel walls. Indeed, the usual chamber pressure of around $5 \cdot 10^{-6}$ mbar might not have been low enough to remove immediately all the water molecules inside the channels [13]. Then, during the initial multiplication phase, these molecules would have first to get ionized by the electron avalanche and removed from the channels by the electric field. The observed time for this initial stabilization phase varies between one and ten minutes. After reaching a peak value,

the current slowly decreases until it stabilizes. This decrease is suspected to be related to charging effects inside the decoupling layer. Both anode and the intermediate electrode are kept at ground potential, so any charges generated between these two electrodes are not easily removed. These charges then modify the electric field distribution, consequently influencing electron multiplication. Eventually, an equilibrium is reached where the gain is stable and reproducible. The same phenomenon could be observed during electron beam-induced current measurements (EBIC) of AMCPs. Under strong excitation of the electron beam microscope, the bright signal from the electrons exiting the channels rapidly decreased until the pores eventually appeared completely dark in the area where the beam was focused, meaning no electrons were coming out of the pores anymore. Furthermore, the area stayed dark even when the beam was switched off for several minutes [12]. The effect of potential charging on the gain will be the subject of further studies. A potential solution could be to widen the channel diameter inside the decoupling stack, reducing the possibility of electrons colliding the channel wall in that area. Gain stability measurements have also been conducted on previous AMCP devices [9] and showed a similar initial spike of the output current. However, the current increased again in these samples after a few minutes. This increase was assumed to be related to a voltage rise on the $\mu\text{c-Si}$ based intermediate electrode and was one of the main motivations to implement a chromium-based middle electrode in the new generation of AMCPs. The fact that this effect is no longer observed supports these previous assumptions. In the future, these gain stabilization studies should be extended to include various input fluxes and gain values of the AMCPs.

D. AMCP conductivity

Another critical parameter in the fabrication of AMCP is the conductivity of the amorphous silicon layer. The layer needs to be conductive enough to replenish the lost charges during the multiplication phase but still needs to sustain large bias

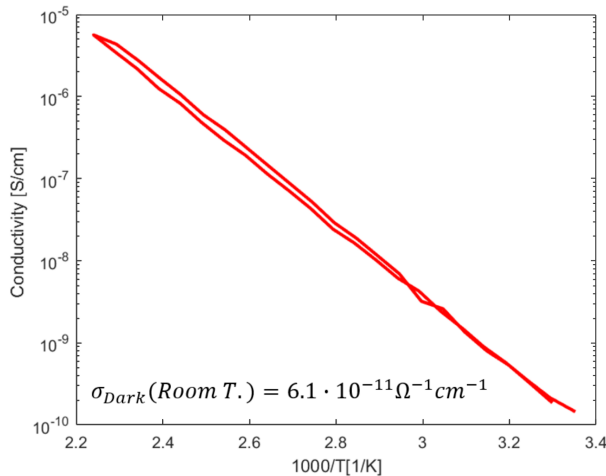


Fig. 7. Arrhenius plot of the dark conductivity of an a-Si:H layer. The conductivity at room temperature was extrapolated from the cooling part of the curve and found to be $\sigma_{dark} = 6.1 \cdot 10^{-11} \Omega^{-1} \text{cm}^{-1}$.

voltages without the risk of causing an electrical breakdown. The dark conductivity of an intrinsic a-Si:H layer strongly depends on the deposition parameters and impurity content and can vary in the range $\sigma_{dark} = 10^{-10} - 10^{-12} \Omega^{-1} \text{cm}^{-1}$ [14]. First, the coplanar dark conductivity of an a-Si:H layer deposited on a glass substrate was measured as a function of temperature under a nitrogen atmosphere of 1 mbar. Two aluminium electrodes were evaporated on the layer for the contacts. The temperature was first increased to 180 °C and then slowly cooled down to ensure the accuracy of the temperature measurement and to guarantee defect thermal equilibrium [14]. The dark conductivity at room temperature was extrapolated from the cooling part of the curve. From this measurement a room temperature conductivity of $\sigma_{dark} = 6.1 \cdot 10^{-11} \Omega^{-1} \text{cm}^{-1}$ was found. The measurement plotted in an Arrhenius plot can be seen in Fig. 7. In the final AMCP device, the conductivity is influenced by the presence of the channels inside the layer. Due to additional localized states existing near the surface of an a-Si:H material, the conductivity can be enhanced in this area. Previous publications already presented an indication of a preferential conduction path along the channel surface [9]. The resistance of the device presented here ("MCP152") was measured to be 35 M Ω . Taking into account the thickness and area of the a-Si:H layer, a conductivity of $\sigma = 2.21 \cdot 10^{-10} \Omega^{-1} \text{cm}^{-1}$ was found, which is about three times larger than the measured dark conductivity in coplanar configuration. This further supports the hypothesis of enhanced conduction along the channel walls. During the operation of the AMCPs, additional effects might influence the resistance, most notably the Poole-Frenkel effect [15], which describes the field-enhanced thermal emission of trapped carriers in a resistive element, or the space-charge-limited current (SCLC) effect [16], [17]. Finally, upon exposure to light, the conductivity of a-Si:H decreases, as expected from the Staebler-Wronski effect (SWE) [18]. This effect is due to an increase in defect density. The induced defects are metastable and can be removed by annealing the material at a high temperature for a

few hours. The conductivity and the resulting resistance of the AMCP directly correlate with the charge replenishment time and, therefore, the maximum count rate. The values found here for the a-Si:H conductivity should therefore serve as a reference point for future optimizations to achieve a fast charge replenishment while still being able to apply high-bias voltages safely.

V. COMPARISON WITH SIMULATIONS

The relationship between gain and bias for the measured channel geometry has also been simulated with a finite element method (FEM) model presented in [19]. Fig. 8 shows the simulated gain compared to the measurements. Under continuous illumination, the measured gain values were of a similar order of magnitude as predicted from the simulation. In this case, the slight deviations can be attributed to the tuning of the model parameters that must be continuously adapted with new experimental data being available. However, the measured gain at weak electric fields was significantly higher under pulsed illumination than the continuous and simulated values, pointing to other physical phenomena being at play. Although this observation can not yet be fully explained, the effect could be related to the presence of the decoupling layer. As mentioned above, charging effects in this area can modify the electric field and hence the measured multiplication gain. This is supported by the fact that no discrepancy between pulsed and continuous gain was observed in alternative prototype AMCPs where the channel diameter was widened inside the decoupling stack (not shown here). With the wider channel opening in this area, the probability of electrons colliding with the channel wall is consequently reduced, meaning charging effects also become less likely [20].

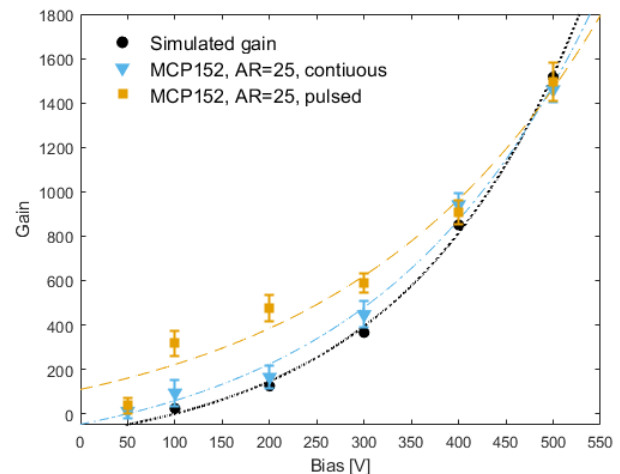


Fig. 8. Simulation of the single channel gain as a function of the applied bias between top and middle electrodes (in absolute value) for the given AMCP geometry with an aspect ratio of 25. Dashed-lines are guides-to-the-eye.

VI. OUTLOOK AND DISCUSSION

The gain values presented above mark a substantial improvement of one order of magnitude compared to previous

generations of the AMCP technology. This opens perspectives for future AMCPs applications. A notable example would be a monolithic integration on top of a CMOS readout, allowed in principle by the processes and low temperature (max. 230 °C) employed here. Nevertheless, there remain several aspects of AMCP stand-alone that can still be improved or clarified.

First, the channel aspect ratios fabricated by deep reactive ion etching have yet to reach their limit. They can still be further pushed to values around 35–40 by optimizing the process parameters. Additionally, channel wall coatings deposited by atomic layer deposition (ALD) also provide a vast potential to increase the AMCP gain further. Early tests with previous AMCPs showed that the gain could be increased by almost a factor of two by using an aluminium oxide coating [9]. This increase could be even higher for magnesium oxide layers due to its high secondary emission yield [21].

Second, in the current devices, the open area ratio of the sensors reaches only about 5% due to the small channel openings (around 1 μm) and minimum pitches of 3 μm (centre-to-centre). Increasing the former would result in a lower gain, and decreasing the latter could affect the structure's stability, demanding other improvement strategies. Preliminary results have shown the possibility of implementing funnel-shaped channel openings (Fig. 9) to maximize the sensors OAR [20]. Additionally, having funnel-shaped AMCPs would also decrease the relative amount of electrons passing straight through or colliding deep inside the channels, effectively solving the issue of the non-tilted channels. Functional funnel AMCPs will be fabricated and studied in the future to assess the improved detection efficiency provided by this strategy.

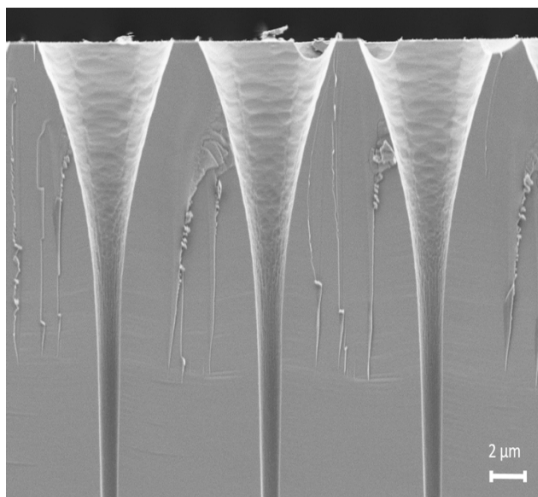


Fig. 9. Microscope image of channels with a funnel-shaped opening. Implementing this funnel geometry in future devices will significantly increase the active area of the AMCPs.

Third, the measurement conditions must be expanded to include larger incoming currents in future experiments. Saturation effects should start to be observable once the current needed to replenish the charges in the channels is of a similar value to the one flowing through the stack (leakage current). Tuning the a-Si:H layer's conductivity could minimize these saturation effects, giving AMCPs an advantage over standard

MCPs in this regard. However, this approach still needs to be investigated and demonstrated. By having a fast charge replenishment, AMCP could be envisioned for applications where high count rates are required. For this purpose, as already mentioned above, it would be helpful to equip the characterization setup with a conventional MCP serving as a pre-amplifier for testing the AMCP saturation under much higher incoming fluxes. This would allow testing the relationship between the detector saturation, the incoming photoelectron flux, and the a-Si:H conductivity. Having a higher input current for the characterization would also reduce the calibration errors of the incoming flux and allow us to quantify the single channel gain more accurately.

Finally, other important metrics, such as the dark count rate and detection efficiency still need to be investigated. Characterizing these values will provide a complete picture of the AMCP's properties and help to evaluate the best-suited applications.

VII. CONCLUSION

In this publication, we presented the fabrication and characterization of the newest generation of AMCPs. One of the main focuses for this new generation was optimizing the fabrication processes. In particular, the a-Si:H deposition by PE-CVD was improved to avoid structural defects in the layer. This allowed for applying higher bias voltages over the channels, which is crucial for achieving a high multiplication factor. By combining photo-lithographic and DRIE processes, channel diameters as small as 1.6 μm and length of 40 μm were realized. Therefore, compared to previous generations of AMCPs [12], the aspect ratio was improved from 13.6 to 25, and the average channel gain increased by an order of magnitude from about 100 to 1500. Another aspect that was improved is the stability of the gain. In earlier AMCP devices, a voltage rise over the intermediate electrode was detected during the multiplication phase, eventually causing an unstable gain [9]. With the introduction of the more conductive chromium-based intermediate electrode, this effect was no longer observed, resulting in a more reproducible gain over time. The AMCPs were characterized under both continuous and pulsed illumination. No saturation effects could be observed under the current measurement conditions, and no significant difference in the maximum gain was measured for the two regimes. The dark conductivity of the a-Si:H multiplication layer has been characterized and hints towards an increased conduction along the channels than in the bulk of the material. The high gain values presented open perspectives for (monolithic) integration of AMCPs with readout circuits. In this view, additional process developments to further improve the gain and collection efficiency have been discussed.

ACKNOWLEDGMENT

The authors would like to acknowledge the staff members of the Center of MicroNanoTechnology (CMi) for their help in optimizing the cleanroom processes that made the fabrication of these devices possible. We are also grateful to all our colleagues at PV-Lab for their input and moral support.

REFERENCES

- [1] J. L. Wiza, "Microchannel plate detectors," *Nucl. Instrum. Methods*, vol. 162, no. 1-3, pp. 587–601, 1979.
- [2] J. Va`vra, D. Leith, B. Ratcliff, E. Ramberg, M. Albrow, A. Ronzhin, C. Ertley, T. Natoli, E. May, and K. Byrum, "Beam test of a Time-of-Flight detector prototype," *Nuclear Instruments and Methods in Physics Research Section A: Accelerators, Spectrometers, Detectors and Associated Equipment*, vol. 606, no. 3, pp. 404–410, Jul. 2009. [Online]. Available: <https://linkinghub.elsevier.com/retrieve/pii/S0168900209008924>
- [3] O. H. W. Siegmund, N. Richner, G. Gunjala, J. B. McPhate, A. S. Tremsin, H. J. Frisch, J. Elam, A. Mane, R. Wagner, and C. A. Craven, "Performance characteristics of atomic layer functionalized microchannel plates," in *UV, X-Ray, and Gamma-Ray Space Instrumentation for Astronomy XVIII*, vol. 8859. SPIE, 2013, pp. 263–274.
- [4] M. A. Popecki, B. Adams, C. A. Craven, T. Cremer, M. R. Foley, A. Lyashenko, A. O'Mahony, M. J. Minot, M. Aviles, J. L. Bond, M. E. Stochaj, W. Worstell, J. W. Elam, A. U. Mane, O. H. W. Siegmund, C. Ertley, L. M. Kistler, and M. S. Granoff, "Microchannel plate fabrication using glass capillary arrays with Atomic Layer Deposition films for resistance and gain," *Journal of Geophysical Research: Space Physics*, vol. 121, no. 8, pp. 7449–7460, Aug. 2016. [Online]. Available: <https://onlinelibrary.wiley.com/doi/abs/10.1002/2016JA022580>
- [5] N. Wyrsh, F. Powolny, M. Despeisse, S. Dunand, P. Jarron, and C. Ballif, "Micro-channel plate detectors based on hydrogenated amorphous silicon," in *MRS Online Proceedings Library (OPL)*, vol. 1245, 2010, publisher: Cambridge University Press.
- [6] P. Shikhaliev, "Saturation model for secondary electron multiplier detectors," *Nuclear Instruments and Methods in Physics Research Section A: Accelerators, Spectrometers, Detectors and Associated Equipment*, vol. 420, no. 1-2, pp. 202–212, Jan. 1999. [Online]. Available: <https://linkinghub.elsevier.com/retrieve/pii/S0168900298008936>
- [7] A. Franco, J. Geissbühler, N. Wyrsh, and C. Ballif, "Fabrication and characterization of monolithically integrated microchannel plates based on amorphous silicon," *Scientific Reports*, vol. 4, no. 1, p. 4597, Apr. 2014, number: 1 Publisher: Nature Publishing Group. [Online]. Available: <https://www.nature.com/articles/srep04597>
- [8] J. Löffler, C. Ballif, and N. Wyrsh, "Amorphous silicon-based micro-channel plate detectors with high multiplication gain," *Nuclear Instruments and Methods in Physics Research Section A: Accelerators, Spectrometers, Detectors and Associated Equipment*, vol. 912, pp. 343–346, Dec. 2018. [Online]. Available: <https://linkinghub.elsevier.com/retrieve/pii/S0168900217314262>
- [9] A. Franco, "Monolithic Particle Detectors based on Hydrogenated Amorphous Silicon," Ph.D. dissertation, EPFL, Lausanne, 2014.
- [10] R. A. Street, "Thermal generation currents in hydrogenated amorphous silicon $p-i-n$ structures," *Applied Physics Letters*, vol. 57, no. 13, pp. 1334–1336, Sep. 1990. [Online]. Available: <https://pubs.aip.org/aip/apl/article/57/13/1334-1336/57378>
- [11] E. H. Eberhardt, "Gain model for microchannel plates," *Applied Optics*, vol. 18, no. 9, pp. 1418–1423, May 1979, publisher: Optica Publishing Group. [Online]. Available: <https://opg.optica.org/ao/abstract.cfm?uri=ao-18-9-1418>
- [12] S. Frey, J. Löffler, C. Ballif, and N. Wyrsh, "Characterization of Amorphous Silicon Based Microchannel Plates with High Aspect Ratio," in *2019 IEEE Nuclear Science Symposium and Medical Imaging Conference (NSS/MIC)*, Oct. 2019, pp. 1–5, ISSN: 2577-0829.
- [13] H. Fritzsche and C. Tsai, "Porosity and oxidation of amorphous silicon films prepared by evaporation, sputtering and plasma-deposition," *Solar Energy Materials*, vol. 1, no. 5-6, pp. 471–479, Jun. 1979. [Online]. Available: <https://linkinghub.elsevier.com/retrieve/pii/0165163379900121>
- [14] A. Shah, *Thin-Film Silicon Solar Cells*. EPFL Press, Aug. 2010, google-Books-ID: DBSkX6w0rFMC.
- [15] J. Frenkel, "On Pre-Breakdown Phenomena in Insulators and Electronic Semi-Conductors," *Physical Review*, vol. 54, no. 8, pp. 647–648, Oct. 1938. [Online]. Available: <https://link.aps.org/doi/10.1103/PhysRev.54.647>
- [16] K. D. Mackenzie, P. L. Comber, and W. E. Spear, "The density of states in amorphous silicon determined by space-charge-limited current measurements," *Philosophical Magazine B*, vol. 46, no. 4, pp. 377–389, 1982, publisher: Taylor & Francis.
- [17] R. L. Weisfield, "Space-charge-limited currents: Refinements in analysis and applications to $a-Si_{1-x}Ge_x:H$ alloys," *Journal of Applied Physics*, vol. 54, no. 11, pp. 6401–6416, Nov. 1983. [Online]. Available: <https://pubs.aip.org/aip/jap/article/54/11/6401-6416/13359>
- [18] D. L. Staebler and C. R. Wronski, "Reversible conductivity changes in discharge-produced amorphous Si," *Applied Physics Letters*, vol. 31, no. 4, pp. 292–294, Aug. 1977. [Online]. Available: <https://pubs.aip.org/aip/apl/article/31/4/292-294/1023070>
- [19] J. Löffler, J. Thomet, S. Frey, C. Ballif, and N. Wyrsh, "Single photon detection with amorphous silicon-based microchannel plates: A Monte Carlo model," *Nuclear Instruments and Methods in Physics Research Section A: Accelerators, Spectrometers, Detectors and Associated Equipment*, vol. 1032, p. 166589, Jun. 2022. [Online]. Available: <https://linkinghub.elsevier.com/retrieve/pii/S0168900222001814>
- [20] S. A. Frey, "Amorphous Silicon Based Microchannel Plates for Time-of-Flight Positron Emission Tomography," Ph.D. dissertation, EPFL, Lausanne, 2023.
- [21] S. J. Jokela, I. V. Vervovkin, A. V. Zinovev, J. W. Elam, A. U. Mane, Q. Peng, and Z. Insepov, "Secondary Electron Yield of Emissive Materials for Large-Area Micro-Channel Plate Detectors: Surface Composition and Film Thickness Dependencies," *Physics Procedia*, vol. 37, pp. 740–747, 2012. [Online]. Available: <https://linkinghub.elsevier.com/retrieve/pii/S1875389212017567>